Weather and Climate Extremes 51 (2026) 100847

Contents lists available at ScienceDirect

Weather and Climate Extremes

journal homepage: www.elsevier.com/locate/wace

Quantifying the spatial extent and attenuation of lake thermal regulation at diurnal scales under extreme heat

Zikang Xing [a], Yunliang Li [a,*], Yufeng Dai [b,**], Jianhui Wei [c], Miaomiao Ma [d], Xuejun Zhang [d], Hui Gao [d], Harald Kunstmann [c,e,f]

[a] State Key Laboratory of Lake and Watershed Science for Water Security, Nanjing Institute of Geography and Limnology, Chinese Academy of Sciences, Nanjing, China
[b] State Key Laboratory of Tibetan Plateau Earth System, Environment and Resources, Institute of Tibetan Plateau Research, Chinese Academy of Sciences, Beijing, China
[c] Institute of Meteorology and Climate Research (IMK-IFU), Karlsruhe Institute of Technology, Campus Alpin, Garmisch-Partenkirchen, Germany
[d] Research Center on Flood and Drought Disaster Reduction of the Ministry of Water Resources, China Institute of Water Resources and Hydropower Research, Beijing, China
[e] Institute of Geography, University of Augsburg, Augsburg, Germany
[f] Centre for Climate Resilience, University of Augsburg, Augsburg, Germany

ARTICLE INFO

Keywords:
Extreme heat
Lake-atmosphere interaction
Lake regulation
Attenuation process
WRF model

ABSTRACT

Lakes worldwide are experiencing intensifying extreme heat, with escalating ecological impacts. Despite lakes' role as thermal buffers to modulate air temperature is well-documented, the spatial propagation dynamics of lake effects remain poorly understood due to complex interactions of lake-atmosphere. This study proposes a synergistic WRF modeling and directional buffer analysis framework to investigate the spatial propagation dynamics and underlying physical mechanisms of lake-induced thermal regulation during extreme heat, focusing on Poyang Lake, China's largest freshwater lake. The results demonstrate a pronounced diurnal asymmetry in lake-induced thermal effects, with distinct spatial propagation characteristics between daytime and nighttime periods. Daytime cooling exhibits an intensity of −1.16 °C, with its influence confined within a 40 km radius, showing a relatively rapid attenuation rate of 0.28 °C per 10 km. In contrast, nighttime warming (+0.97 °C) propagates 1.75 times farther than its daytime counterpart, extending up to 70 km downwind while maintaining a slower attenuation rate of 0.13 °C per 10 km. Directional analysis reveals north-oriented propagation of lake thermal effects, influenced by prevailing southerly winds and lake-land breeze. Vertical profile analysis reveals distinct altitudinal penetration of lake-induced thermal effects, with daytime influences confined below 900 hPa while nighttime impacts extend up to 700 hPa. Daytime cooling extent is limited by turbulent mixing, whereas nighttime warming is enhanced by stable air conditioning and advective transport. The study underscores the role of lake-atmosphere interactions in mitigating regional climate extremes, providing critical insights for nature-based heat adaptation strategies in lake-rich regions. These findings advance the understanding of inland water bodies as active climate regulators under anthropogenic warming.

1. Introduction

Anthropogenic climate change has markedly amplified heatwaves globally, which are defined as prolonged periods of abnormally high air temperatures. (Kong et al., 2024; Luo et al., 2024). Recent studies document a threefold increase in heatwave frequency since pre-industrial times, with particularly pronounced intensification during the 2020s (Wei et al., 2020). Terrestrial heatwaves have intensified by 1–3 °C while lasting 45–60 % longer over the past century, creating cascading impacts across ecosystems and societies (Huntingford et al., 2024). The 2022 European event alone resulted in >61,000 heat-related deaths and $20 billion agricultural losses (Cremona et al., 2023), while concurrent record-breaking heat in Southeast China affected 4.08 million ha of cropland and 4.3 million residents (Zhang et al., 2023). In this context, inland water bodies, particularly large lakes, have emerged as critical natural regulators that can mitigate the intensity and spatial extent of extreme heat events through unique lake-atmosphere feedback.

* Corresponding author.
** Corresponding author.
E-mail addresses: yunliangli@niglas.ac.cn (Y. Li), yufengdai@itpcas.ac.cn (Y. Dai).

https://doi.org/10.1016/j.wace.2025.100847
Received 17 August 2025; Received in revised form 15 December 2025; Accepted 15 December 2025
Available online 16 December 2025

Lakes play a pivotal role in modulating regional climate through their distinct thermodynamic and physical properties, which govern land-atmosphere interactions (Adrian et al., 2009; Woolway et al., 2020). Their ability to alter local weather stems from differences in heating between land and water, while their thermal behavior is primarily driven by the atmosphere above (Von Schuckmann et al., 2022). As integral components of the climate system, lakes have characteristics of transparency to solar radiation, low albedo, small momentum roughness length, high thermal conductivity, and large heat capacity relative to the land surface, which enable them to reshape boundary layer dynamics, influence mesoscale circulation, and modify regional heat and moisture budgets (Dai et al., 2020; Sun et al., 2014). While existing research has largely treated lakes as passive indicators (lakes' thermal regimes are driven by climatic forcing) of climate extremes (Wang et al., 2024a,b; Zhou et al., 2023), their active role (modifying regional climate through physical processes) in regulating thermal regimes via lake-atmosphere feedbacks remains underexplored.

Evidence from holistic approaches, such as in situ monitoring, remote sensing, and numerical modeling, has revealed the lake's effect on regional heat budgets and local climate. Regarding observational evidence, a comparative analysis of meteorological records near Lake Sayama (Japan) revealed a 0.46 °C reduction in the August diurnal temperature range between the reservoir's empty and full stages (Ueno and Ohta, 2020). Similarly, by integrating in situ station data with MODIS remote sensing, Li et al. (2019) quantified Qinghai Lake's capacity to delay seasonal temperature maxima by 1.9–10.5 °C. Building on this observational foundation, numerical modeling studies have been instrumental in advancing a process-based understanding of lake-climate interactions across diverse scales. At the regional scale, Zhu et al. (2018) conducted regional climate model experiments for the Tibetan Plateau, demonstrating that lakes exert year-round cooling effects on near-surface air temperature through combined reductions in sensible heat flux (-15 W m^{-2}) and enhanced summer evaporation ($+1.2$ mm day^{-1}). At the global scale, Vanderkelen et al. (2021) utilized the Community Earth System Model to indicate that reservoirs significantly reduce diurnal temperature variability (-0.8 °C) and moderate extreme temperatures. Critically, the integration of lake models into atmospheric dynamic frameworks has emerged as an essential approach for investigating the full spectrum (zero to three-dimensional) physical processes through which lakes regulate extreme heat events (F. Wang et al., 2019; Wang et al., 2022). Despite these advances, fundamental uncertainties persist regarding the three-dimensional trajectories, directional attenuation rates, and dominant physical mechanisms governing the spatial propagation of lake effects under extreme heat.

Although the role of lakes in modulating local and regional climate is well established, the spatial propagation of these regulatory effects exhibits heightened complexity under compounded monsoon and extreme heat forcing. Monsoonal circulation alters thermal advection patterns by disrupting canonical lake-land breeze systems (Tsujimoto and Koike, 2013). For instance, a daytime cooling signal over lakes could stem from either local evaporative processes or the advection of monsoon-cooled air masses (Sun et al., 1997). Concurrently, extreme heat imposes nonlinear thermodynamic constraints (Collazo et al., 2024; Wang et al., 2019). These interacting forcings fundamentally restructure the mechanism of lake-atmosphere exchanges, with monsoons modifying spatial propagation pathways and heatwaves amplifying diurnal asymmetry. This ambiguity highlights the critical need for process-based modeling frameworks to isolate and quantify lake-mediated feedback within these complex, multiscale climate interactions (Bennington et al., 2014).

Studies in this direction have demonstrated that lakes significantly modulate local and downwind climates under monsoon influence through distinct diurnal processes. Evidence demonstrates that lake thermal effects propagate considerable distances (Mishra et al., 2011; Zhang et al., 2021). For example, Taihu Lake's cooling extends 10–20 km during summer (Gu et al., 2016), while Alqueva reservoir's breeze fronts mitigate heat intensity 6 km (Iakunin et al., 2018). Lake Seling Co's cooling effects propagate over 50 km during the South Asian summer monsoon season, sufficient to modify downwind precipitation patterns (Qiu et al., 2023). These findings collectively confirm that lake thermal regulation follows distance-decay dynamics shaped by monsoonal circulation patterns. However, current quantification of the spatial propagation mechanisms remains incomplete, with fundamental uncertainties persisting regarding (1) the three-dimensional trajectories of lake-effect propagation, (2) directional variations in attenuation rates, and (3) the dominant physical mechanisms controlling propagation dynamics. Our study therefore addresses the overarching research question: What are the spatial propagation patterns and underlying physical mechanisms of lake-induced near-surface temperature modification during extreme heat events?

This study regarding lake-atmosphere interaction focuses on Poyang Lake, China's largest freshwater lake, located in the middle reaches of the Yangtze River, within the East Asian monsoon climate zone (Li et al., 2021). Our study area selection is strategically based on three key considerations: (1) As a unique hydro-ecological system, Poyang Lake and its surrounding wetlands provide an ideal natural laboratory for studying lake-atmosphere feedbacks during climatic extremes; (2) The increasing frequency of extreme events, particularly the unprecedented 2022 heatwave, has generated compound ecological impacts including thermal stratification, hypoxia, and ecosystem degradation (Ma and Yuan, 2023); (3) The lake's geomorphology - located in a topographically uniform basin with minimal terrain-induced airflow disturbance - creates an exceptional natural experiment for studying spatial propagation of lake effects (Wei et al., 2020). These conditions collectively present a rare opportunity to investigate lake-mediated climate feedback when both hydrological and atmospheric systems exceed their historical variability ranges.

Thus, the objectives of this study are to: (1) quantify the spatiotemporal patterns of daytime lake cooling and nighttime warming under extreme heat, (2) characterize the propagation dynamics of lake thermal regulation (including horizontal/vertical extent, directional preference, and attenuation processes), and (3) elucidate the underlying physical mechanisms governing these spatial propagation patterns. To achieve these objectives, this study proposes a synergistic WRF modeling and directional buffer analysis framework. The quantified propagation scales provide essential parameters for improving climate model representations of lakes. The findings here advance understanding of how inland waters modulate regional climate extremes, with critical implications for nature-based heat mitigation strategies in lake-rich watersheds.

2. Materials and methods

2.1. Study area

This study examines Poyang Lake (29.2°N, 116.3°E) and its surrounding region (25–31.2°N, 112–120°E), China's largest freshwater lake located in the Yangtze River's middle reaches (Xing et al., 2024). As a floodplain lake, it exhibits pronounced hydrological variability, with an average surface area of 3 500 km^2 and a mean depth of 8.4 m under normal conditions (Li et al., 2020). The lake shows substantial thermal variation (6–30 °C; mean ~ 18 °C). According to 2022 land use data from the ESA CCI-LC dataset, land cover comprises open water (41.8 %), forest (35.3 %), cropland (17 %), urban areas (2.3 %), grassland (3.2 %), and shrubland (0.2 %). The humid subtropical monsoon climate features distinct seasons: hot-humid summers and cool-dry winters, with mean annual precipitation of 1 680 mm (75 % occurring April–September), evaporation of 900 mm, and air temperature of 17.5 °C (Wei et al., 2024).

2.2. Regional climate model

2.2.1. Model configuration

The Weather Research and Forecast model (WRF) version 4.3.3 is employed for our study on modeling lake-induced local climate effects. WRF is a limited-area mesoscale model that simulates a coupled, nonlinear system of the land surface and the atmosphere (Skamarock et al., 2008). A nested two-domain setup (Fig. 1a) is used in this study. The outermost domain (D1) has a horizontal resolution of 30 km with 140 × 140 grid points. The innermost domain (D2) has a horizontal resolution of 5 km with 246 × 246 grid points. An uneven vertical discretization of 38 levels up to 50 hPa for the atmosphere is used for both D1 and D2.

For the selection of the physical schemes of WRF, we closely follow our previous studies of Wei et al. (2024) and Wagner et al. (2016). Specifically, the WRF Single-Moment 5-class scheme (WSM5) is used as a microphysics scheme (Hong et al., 2004), the Yonsei University scheme (YSU) as a planetary boundary layer scheme (Hong et al., 2006), the Noah Land Surface Model as a surface scheme (Chen and Dudhia, 2001), and the revised MM5 Monin–Obukhov scheme as a surface layer (Jiménez et al., 2012). For cumulus parameterization, the Betts–Miller–Janjic (BMJ) scheme (Betts, 1986; Betts and Miller, 1986) is turned on for the D1 and D2 simulations. For the radiation scheme, the Rapid Radiative Transfer Model (RRTM) is used here for longwave radiation (Mlawer et al., 1997) and the Dudhia scheme for shortwave radiation (Dudhia, 1989). On the parameterization of lake thermodynamic processes, the lake model originates from the Community Land Model version 4.5 (Oleson et al., 2013) with modifications by Gu et al. (2015) and is employed in this study. This one-dimensional mass and energy balance model is built upon the Hostetler lake model framework (Hostetler et al., 1993, 1994; Hostetler and Bartlein, 1990).

To minimize the potential bias introduced by lake temperature initialization in the model simulations, we implement a satellite-based correction approach using MODIS Land Surface Temperature (LST) products. The daily MODIS LST data (MOD11A1, Collection 6) at 1 km resolution are spatially averaged over Poyang Lake's water surface area (Wan et al., 2015). These satellite-derived lake surface temperatures are assimilated into the WRF-lake modeling system through a two-step procedure: (1) The initial lake temperature field in WRF is adjusted to match the MODIS LST climatology for the corresponding simulation period; (2) A spin-up period of 30 days is implemented to allow the lake model to reach dynamic equilibrium with the atmospheric forcing while maintaining the satellite-constrained thermal baseline. The assimilation particularly improves the representation of diurnal temperature cycles and spatial thermal gradients across the lake's sub-basins.

2.2.2. Experimental design

In this study, a set of regional dynamic downscaling experiments using WRF are designed to quantify the lake-induced modulation on air temperature. The evaluation simulation (i.e., control simulation, CTRL) for historical periods is conducted adopting 2022 land cover data as its baseline input (Fig. 1c). In contrast, the sensitivity test simulation (i.e., lake-remove simulation, NOLA) modifies the land cover by converting Poyang Lake grid cells into cropland, the predominant land use type in the surrounding region (Fig. 1d). In this experiment, the lake surface area is treated as a static parameter, meaning seasonal variations in lake extent, water storage, and depth are not considered in the simulations. The static lake-removal approach is a well-established and standard sensitivity technique in regional climate modeling designed to isolate the maximum potential climatic impact of the lake by creating a stark contrast. These simplifications allow to clearly attribute any differences in simulation results directly to the presence of the lake surface itself, without the confounding effects of complex land-cover transitions.

The CTRL and NOLA simulations begin at 0 000 UTC on 1 June 2022

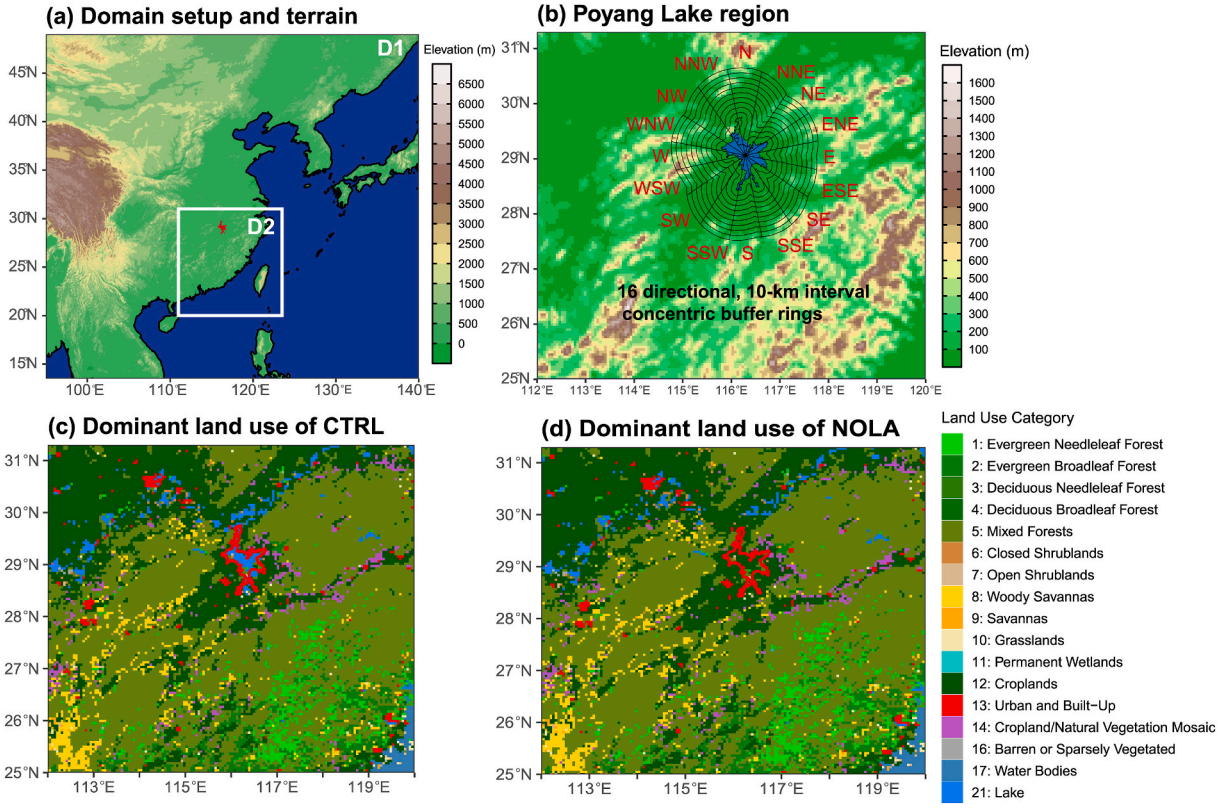

Fig. 1. (a) WRF model domain: the 30-km outer (D1) and 5-km inner (D2) simulation domain. The terrain heights (m) are shown in color. (b) Terrain height of the Poyang Lake region. The blue-shaded area represents Poyang Lake, and the black frame delineates the 16 sectors. 10-km concentric buffer zones are used to quantify the directional characteristics of lake-induced climate effects. (c, d) Land use type in WRF configuration for the CTRL and NOLA scenarios.

and span the period from June to September 2022, capturing the entirety of the unprecedented 2022 Yangtze River Basin heatwave. This event, characterized by temperatures exceeding 40 °C for multiple consecutive days across the region, represents one of the most severe heatwaves in at least six decades, with its intensity quantitatively estimated as approximately a 1-in-64-year event relative to the 1979–2014 climate (Ma and Yuan, 2023). The forcing data is taken from the state-of-the-art global reanalysis provided by the European Center for Medium-Range Weather Forecasts, ECMWF, namely ERA5 (Hersbach et al., 2020). ERA5 provides hourly atmospheric, oceanic, and land-surface variables at a horizontal resolution of 0.25° × 0.25° for the globe from 1940 until the present.

The WRF model incorporates the Noah-modified 21-category IGBP-MODIS land cover classification scheme to characterize land cover types and associated surface parameters such as albedo, leaf area index, and vegetation fraction. However, research has shown that the model's default surface data may not accurately reflect real-time land cover conditions (Jach et al., 2020; Wang et al., 2023). To address this limitation, this study replace the default land use data with higher-resolution (300 m) satellite-derived land cover information from the European Space Agency's Climate Change Initiative (CCI-LC) dataset (Defourny et al., 2017). For the NOLA simulation, key surface parameters (albedo, leaf area index, and vegetation fraction) are uniformly adjusted to match the average values of adjacent cropland areas, effectively simulating the hypothetical disappearance of the lake.

2.2.3. Reference data and validation strategy

For the performance assessment of the historical simulations, the ERA5-Land reference data set of historically 2-m air temperature (T_a) is used. ERA5-Land (Muñoz Sabater, 2019; Muñoz-Sabater et al., 2021) is an enhanced global gridded dataset (with horizontal resolution of 10 km) for the land component of ERA5 produced by ECMWF, spanning 1950 to the present day with hourly resolution. The ERA5-Land dataset incorporates the FLake model (Rooney and Bornemann, 2013), explicitly accounting for lake effects in its land-surface and meteorological variables. To facilitate the comparison of the simulations to the reference data, the bilinear interpolation method is employed to resample the WRF-simulated T_a to the reference data grids.

In addition, daily mean T_a observations from three meteorological stations (Lushan, Jingdezhen, and Changbei) around Poyang Lake are collected for independent model validation. These observations are collected by the China Meteorological Administration. The geographical locations and metadata of these stations are provided in Supplementary Table S1 and Fig. S1. These in-situ measurements serve as fully independent ground-truth data to robustly assess the model's performance.

Four statistical metrics, namely, spatial correlation coefficient (SCC), Pearson's correlation coefficient (PCC), Mean relative bias (MRB), and Root mean square error (RMSE) with a calculated p value (the significance level of 99 %), are used to quantify the performance of the WRF Model in terms of reproducing spatial patterns and temporal variation of T_a of the reference.

2.3. Detection of lake-induced thermal regulation

To systematically evaluate the spatial propagation of lake-induced thermal effects, we analyze air temperature modifications (ΔT_a) during typical daytime hour (15:00 local time) and typical nighttime hour (06:00 local time). These specific hours are selected as they represent the daily maximum (15:00) and minimum (06:00) air temperature in this region, when lake thermal effects are most pronounced. The lake-affected area (% of study area) is quantified as the percentage of the study domain exhibiting statistically significant cooling ($\Delta T_a > 0, p < 0.05$) during daytime or warming ($\Delta T_a < 0, p < 0.05$) during nighttime relative to NOLA reference conditions. The significance level of ΔT_a at each grid cell is calculated using a two-sided Student's t-test based on daily time series. Correspondingly, the magnitude of lake thermal regulation is calculated as the mean ΔT_a across all significantly modified grid cells within the affected area.

A directional buffer analysis framework is implemented to quantify the anisotropic propagation of lake-induced thermal effects by establishing 10-km concentric zones radiating from Poyang Lake's shoreline (Fig. 1b), divided into 16 azimuthal sectors with 22.5° resolution. Mean ΔT_a values are calculated for each buffer ring through radial averaging, generating directional ΔT_a-distance curves that reveal the spatial decay patterns of lake influence. Statistically significant turning points in these curves are identified using piecewise regression analysis, with turning points objectively marking the transition from lake-dominated to background thermal regimes based on criteria of $p < 0.01$ for slope changes. Three key metrics are derived to characterize the lake's thermal regulation: the mean ΔT_a within the directional zone represents the thermal intensity, the distance between the turning point and the lake boundary quantifies the maximum propagation range, and the ΔT_a gradient between the lake boundary and the turning point measures the attenuation efficiency. This comprehensive approach enables systematic evaluation of how lake thermal effects vary across directions and provides standardized metrics for comparing thermal propagation characteristics under different meteorological conditions.

3. Results

3.1. Model evaluation

This section evaluates the WRF model's performance in reproducing T_a pattern across the study area relative to reference data. Fig. 2 presents the spatial distribution of T_a for the entire simulation period, typical daytime hour, and typical nighttime, comparing CTRL simulation results (left) with ERA5-Land data (middle) and their differences (right) for the Poyang Lake region. The results indicate that the WRF model demonstrates good skill in reproducing the observed northwest-to-southeast T_a gradient (SCC = 0.73, Table 1). However, a systematic cold bias is evident (MRB = −2.98 %), with consistent error patterns across all periods. Negative biases predominantly occur in the eastern mountainous areas, while positive biases appear over the central and southwestern plains. The topographic correspondence suggests that terrain complexity contributes to the cold bias, particularly in southern highlands.

Notably, the model shows better nighttime performance (MRB = −2.29 %, RMSE = 1.42 °C) than daytime simulations (MRB = −3.51 %, RMSE = 2.30 °C), with daytime errors primarily stemming from underestimated temperatures in the southwestern mountains. The simulation accurately reproduces both the daytime cooling and nighttime warming effects around Poyang Lake, with spatial patterns and magnitudes closely matching reference data. These results confirm the model configuration's suitability for investigating lake-atmosphere interactions.

To further evaluate the model's performance against independent observations and address potential biases from using reanalysis data, we validate the simulated daily mean T_a against measurements from three meteorological stations (Lushan, Jingdezhen, and Changbei; Supplementary Fig. S1). The results demonstrate that the WRF model successfully captures the observed daily variations and amplitude of T_a during the 2022 extreme heat event. This is evidenced by a strong agreement with station observations, yielding a mean PCC of 0.78 ($p < 0.01$), a mean MRB of −3.54 %, and a mean RMSE of 2.30 °C. This independent verification strengthens confidence in the model's reliability for reproducing temporal dynamics of T_a.

3.2. Spatial propagation of lake thermal effect

This section investigates the spatiotemporal characteristics of lake-induced air temperature alteration (ΔT_a). The examination begins with a detailed assessment of horizontal distribution patterns across the

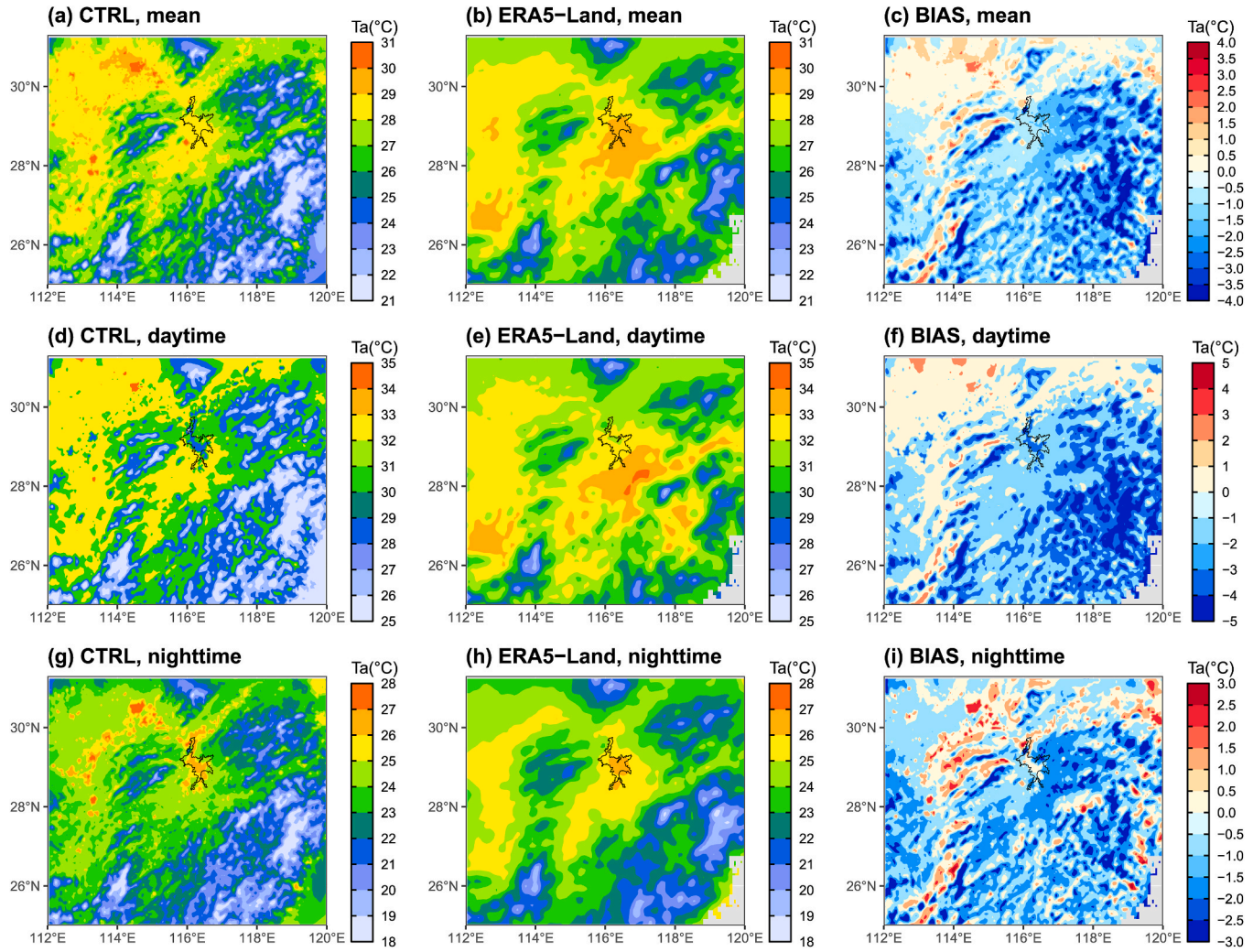

Fig. 2. Spatial distributions of average T_a during (a–c) the entire simulation period, (d–f) typical daytime hour (15:00 local time), and (g–i) typical nighttime hour (06:00 local time) from the CTRL simulations (left column: a, d, and g) and ERA5-Land dataset (center column: b, e, and h). (right column: c, f, and i) The corresponding differences of T_a between the CTRL simulation and the ERA5-Land dataset. The black frame represents the boundary of Poyang Lake.

Table 1
Performance metrics evaluating the WRF-simulated T_a against reference data.

Metrics	Daily mean	Daytime	Nighttime
SCC	0.73**	0.64**	0.75**
PCC	0.83**	0.78**	0.87**
MRB	−2.98 %	−3.51 %	−2.29 %
RMSE	1.73 °C	2.30 °C	1.42 °C

**$p < 0.01$.

study domain, revealing distinct thermal anomalies centered over Poyang Lake and its immediate surroundings. Fig. 3 reveals pronounced daytime cooling (−2.6 °C) and nighttime warming (+2.8 °C) effects, with maximum thermal changes occurring directly over Poyang Lake. Significance tests indicate the nighttime warming area substantially exceeds the daytime cooling extent. The cooling effect is primarily confined to airspaces above the lake and adjacent Yangtze River floodplains to the west and northeast. The Lushan Mountains divide the eastern and central cooling zones into two distinct regions. In contrast, the nighttime warming pattern shows continuous spatial coherence.

From a latitudinal-longitudinal perspective, the ΔT_a distributions exhibit single-peak patterns centered over Poyang Lake in the zonal direction, while exhibiting multimodal structures with multiple variation points along the meridional transect that extend beyond the immediate lake vicinity. Both the cooling and warming effects exhibit a clear spatial decay pattern with increasing distance from the lake, as evident from the longitudinal and latitudinal mean profiles.

Fig. 4 displays the west-east vertical cross-section of lake-induced ΔT_a along 29°N, demonstrating Poyang Lake's significant influence on the three-dimensional structure of lake-atmosphere interactions. The lake's thermal modulation weakens progressively with height. During daytime, substantial cooling penetrates up to 900 hPa, primarily confined vertically above the lake surface. Notably, an additional cooling layer emerges above 600 hPa, though isolated from the surface-driven cooling by an intervening warm layer. Nighttime conditions exhibit contrasting patterns, with warming extending beyond 800 hPa across broad regions east and west of the lake, while a distinct cold layer forms above 700 hPa. Comparative analysis reveals a persistent memory effect in the 900-400 hPa layer, characterized by consistent lower-level warming and upper-level cooling. This elevated warming layer notably constrains the vertical extent of daytime cooling below 900 hPa.

Further investigation of temporal variations in lake-affected area and intensity (Fig. 5) reveals consistent diurnal patterns between the spatial extent and magnitude of lake effects, indicating strong coupling between these parameters. The 15-day moving average effectively filters high-frequency variability and reveals underlying temporal trends. The daytime cooling effect intensifies progressively from June to August, peaking in mid-July and late August (−0.94 °C, 73 % coverage), before

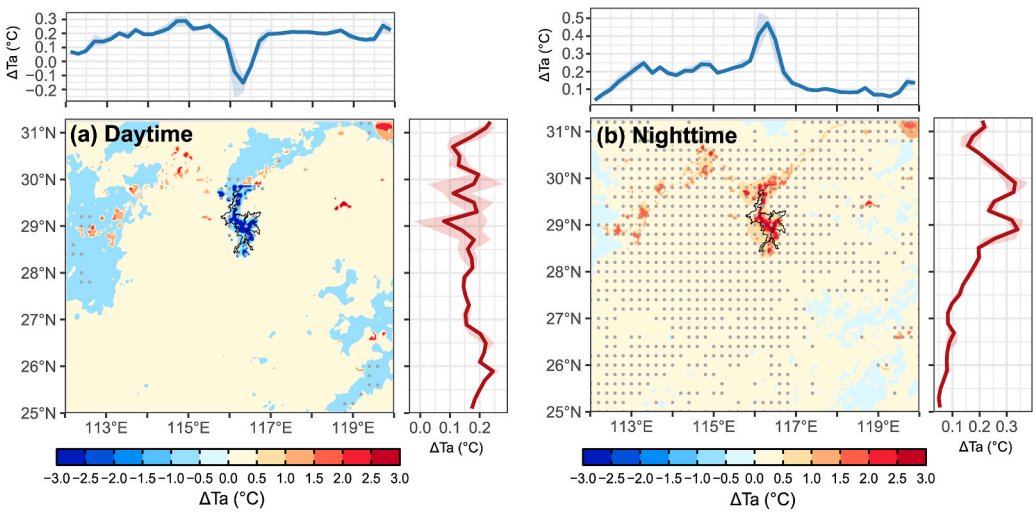

Fig. 3. Spatial distributions of lake-induced average ΔT_a (CTRL minus NOLA) at (a) typical daytime hour (15:00 local time) and (b) typical nighttime hour (06:00 local time). Longitudinal (top) and latitudinal (right) mean profiles are shown with 0.25° binning, with the shaded region representing the variability of ΔT_a. Dots denote grid cells where differences are significant at the 95 % significance level using a two-sided Student's *t*-test based on daily time series. The black frame outlines the boundary of Poyang Lake. All values represent the average differences during the simulation.

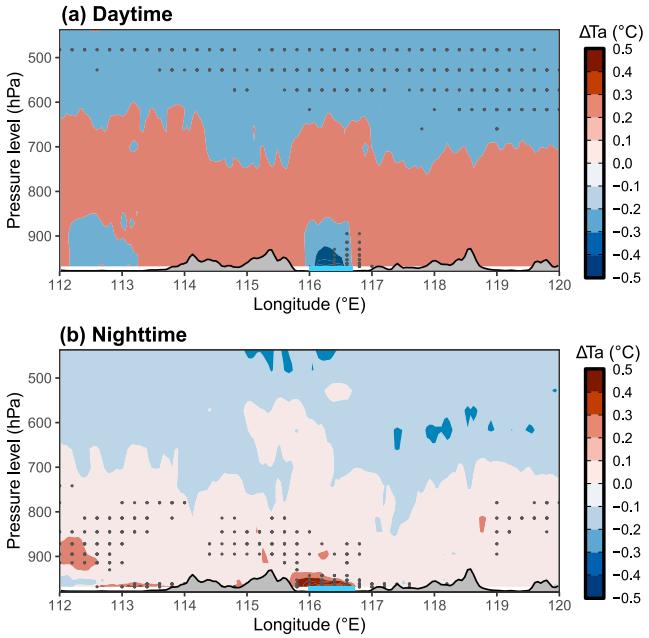

Fig. 4. West-East cross section at 29°N of lake-induced average ΔT_a (CTRL minus NOLA) at (a) typical daytime hour (15:00 local time) and (b) typical nighttime hour (06:00 local time). Dots denote grid cells where differences are significant at the 95 % significance level using a two-sided Student's *t*-test based on daily time series. All values represent the average differences during the simulation. The gray shaded area represents the terrain height, and the blue bold line denotes the location of Poyang Lake.

weakening in September. In contrast, nighttime warming of the lake follows a distinct temporal progression, with gradual intensification through June–August and maximum values occurring in September (1.02 °C, 79 % coverage).

Using the directional buffer analysis framework, lake-induced ΔT_a across varying distances and directions is quantified. The distance-ΔT_a relationship curves averaged on all directions exhibit distinct significant turning points for both daytime and nighttime (Fig. 6). On the inner side of these turning points, ΔT_a demonstrates monotonic decay as distance from the lake increases, with the thermal influence gradually diminishing at a rate of approximately 0.2 °C per 10 km. This decay pattern reflects the progressive dissipation of lake-induced thermal effects through atmospheric mixing and energy exchange with the surrounding land surface. In contrast, the outer side of the turning points shows statistically stable ΔT_a that remain nearly constant with further distance increases, indicating the transition to background atmospheric conditions where lake influence becomes negligible. The turning points mark critical thresholds in the spatial propagation of lake effects, representing the maximum extent where lake-induced thermal modifications remain detectable above natural variability.

This characteristic two-phase relationship remains robust across all 16 directional sectors (Supplementary Figs. S3–S4), consistently demonstrating the distinct spatial decay pattern of lake thermal influence. However, two notable exceptions emerge in the NNE and NW sectors, where secondary inflection points are detected in addition to the primary transition points that are annotated in the analysis.Fig. 6 also presents compelling evidence of directional variability in the spatial attenuation of lake-induced thermal effects through boxplot analysis. This directional dependence is most pronounced within the first 20 km from the shoreline. Beyond the identified turning points, the analysis demonstrates a consistent convergence of ΔT_a values toward spatial uniformity across all directions, indicating the gradual dissipation of directional influences with increasing distance from the lake.

The distance-decay characteristics of lake-induced thermal effects exhibit marked diurnal asymmetry, with turning points identified at 40 km (daytime) and 70 km (nighttime). This spatial pattern indicates significantly faster attenuation of daytime cooling effects compared to nighttime warming. The rapid daytime attenuation within 40 km primarily results from strong thermal forcing by the warmer surrounding land surface, where the lake's limited cooling capacity is quickly overwhelmed by ambient heat conditions. At the turning point, the daytime ΔT_a shows an increase of 1.16 °C relative to the lake center. In contrast, nighttime ΔT_a shows a reduction of 0.97 °C. The observed decay rates also show diurnal asymmetry, with steeper gradients during daytime (0.28 °C/10 km) compared to nighttime (0.13 °C/10 km).

Sensitivity analyses (Supplementary Fig. S2, Fig. S5-S10) are conducted to test the robustness of the identified turning points (40 km for daytime, 70 km for nighttime) against methodological choices. Variations in buffer width (5, 10, and 15 km) resulted in deviations within ±5 km for both daytime and nighttime distances. Similarly, altering the sector numbers (8, 16, and 32) has a negligible impact on the mean ΔT_a-distance curves. A higher sector number (e.g., 32) provided a more

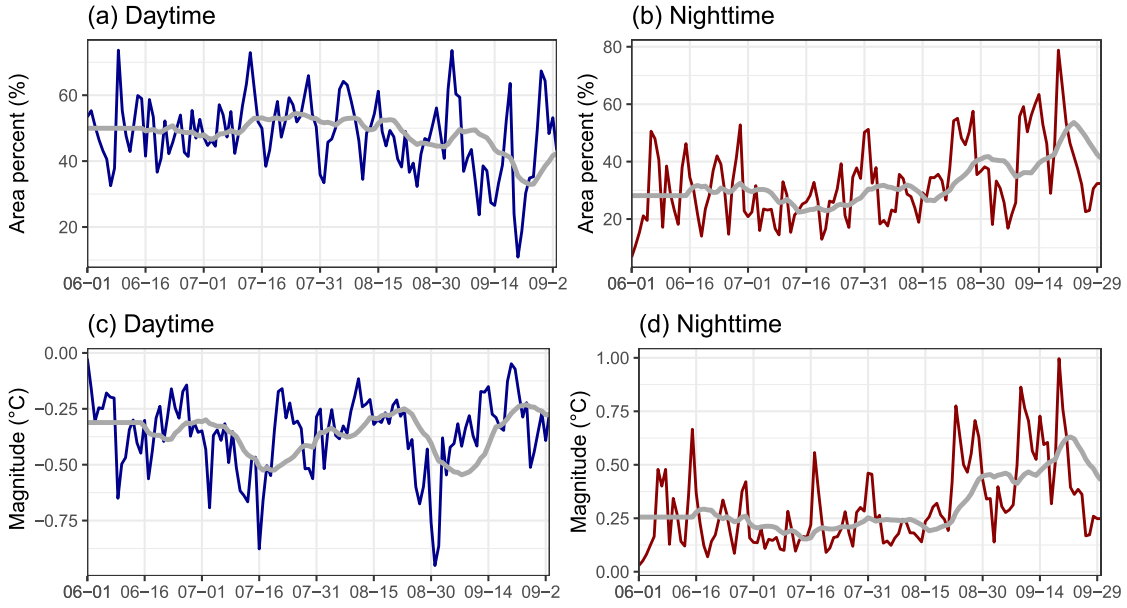

Fig. 5. Temporal variation in (a, b) lake-affected area (% of study area) and (c, d) influence magnitude (°C) at (left column) typical daytime hour (15:00 local time) and (right column) typical nighttime hour (06:00 local time). Gray lines refer to the 15-day moving average.

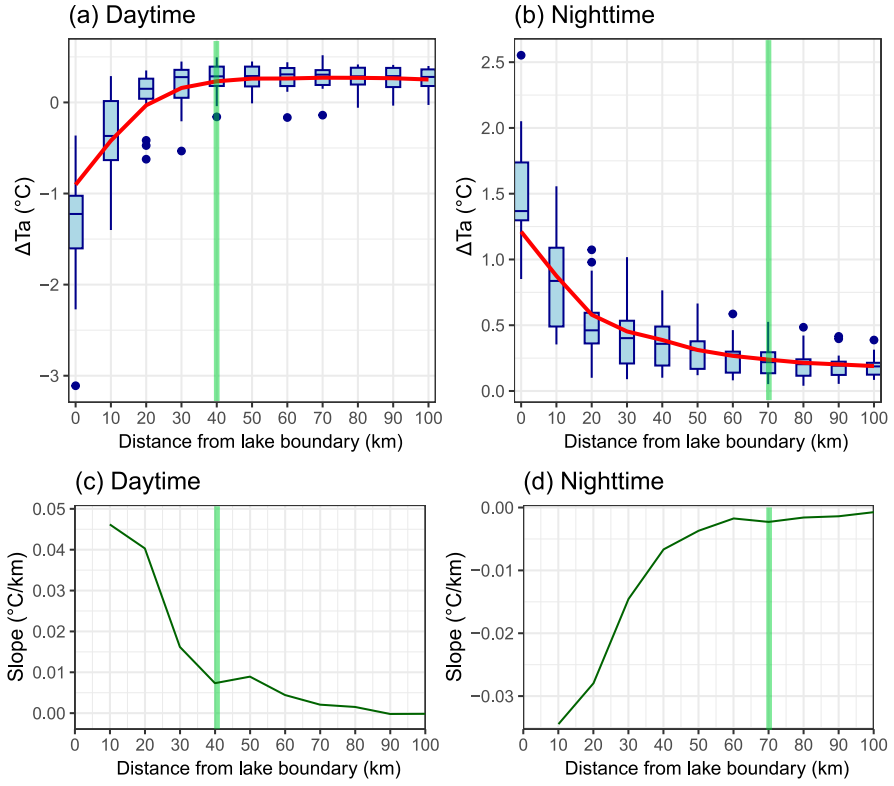

Fig. 6. Distributions of (a, b) lake-induced ΔT_a and (c, d) their corresponding distance-dependent gradients along the distance from lake boundary at (a, c) typical daytime hour (15:00 local time) and (b, d) typical nighttime hour (06:00 local time). Zero distance denotes ΔT_a over Poyang Lake. Boxplot display directional variability, with the blue solid line and the boxes representing the multi-directional mean and ±1σ variability, respectively. Outliers are shown as individual points. Green lines refer to turning points.

detailed representation of the ΔT_a distribution within 0–30 km. The 10-km buffer combined with the 16-sector setup is ultimately selected as it offers an optimal balance between capturing spatial detail and maintaining statistical stability.

To systematically quantify the directional dependence of lake-induced thermal attenuation, three parameters are analyzed across 16 directions for both daytime and nighttime: mean ΔT_a magnitude, turning point distance derived from ΔT_a-distance curves, and ΔT_a

change from lake boundary to turning point. Distinct diurnal patterns emerge in the directional distributions (Fig. 7). Daytime cooling exhibits a cross-shaped spatial pattern in mean ΔT_a magnitude, without clear directional dominance (Fig. 7a–b). However, the turning point distances reveal obvious north-south propagation of cooling effects, with maximum extension along the NNW direction (60 km, Fig. 7c). Nighttime warming shows analogous directional preference, also following the north-south orientation (max distance is 80 km, Fig. 7d).

The daytime ΔT_a increase and nighttime ΔT_a decrease from lake center to turning point demonstrates stronger directional variability (Fig. 7e–f). The change of ΔT_a is primarily distributed in the southwest direction, with notable extensions along the WSW, SE, and E directions, a pattern consistent for both daytime and nighttime. The directional distribution of ΔT_a change does not align with the turning point distances, indicating that the intensity and spatial extent of lake effects vary independently across different directions. In summary, the spatial

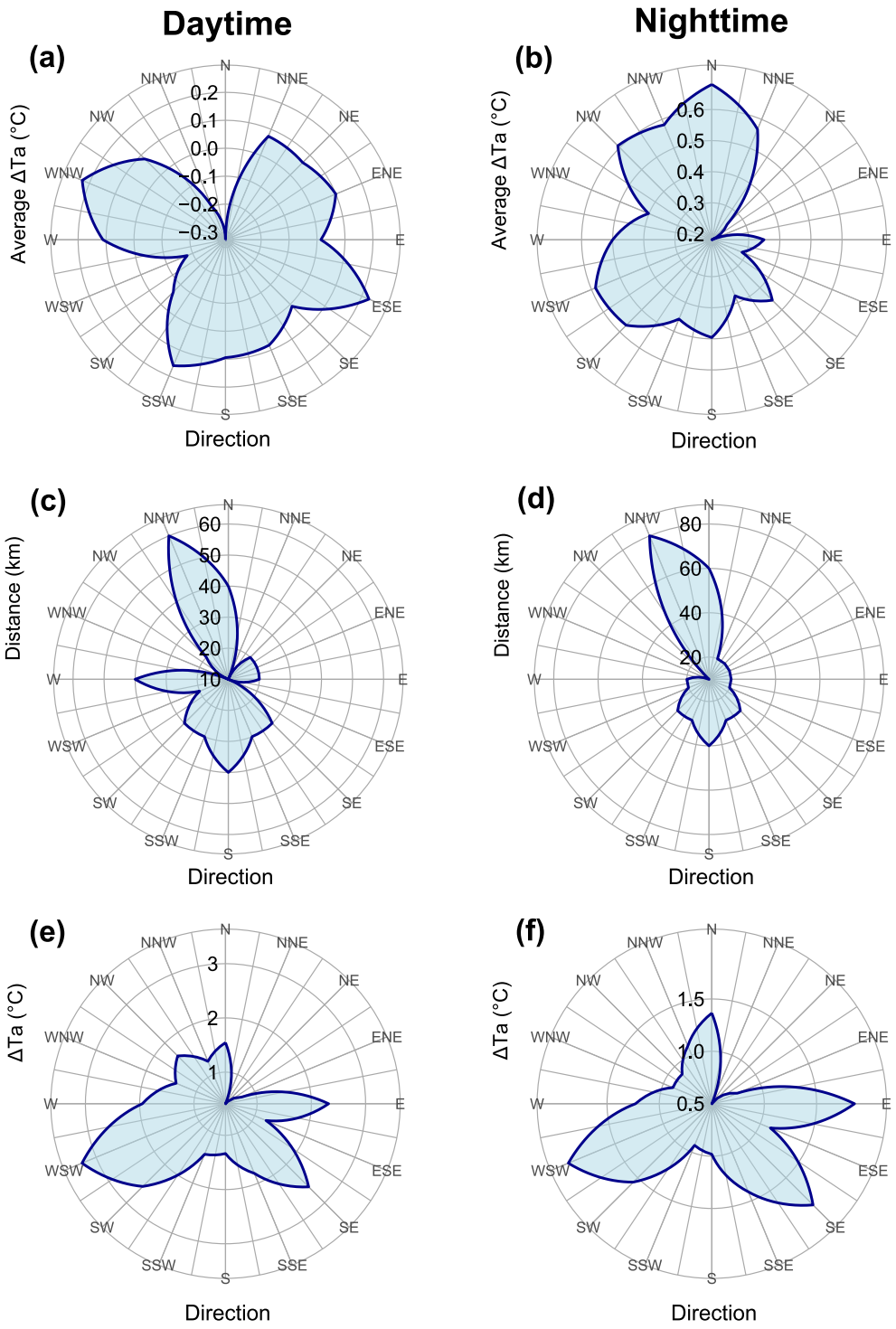

Fig. 7. Radar plots showing the directional distribution (16 sectors) of lake-induced cooling or warming effects at typical daytime hour (left) and typical nighttime hour (right): (a, b) mean ΔT_a of different directions; (c, d) inflection point distance derived from ΔT_a-distance curves; (e, f) ΔT_a decrease (or increase) from inflection point to lake center. Since values in (f) are negative, their absolute values are plotted for clearer visualization.

propagation of lake-induced thermal regulation exhibits significant directional heterogeneity.

The spatial dissociation between the maximum intensity and the maximum propagation distance of lake-induced ΔT_a reveals the distinct roles of local thermodynamics versus regional dynamics. The strongest cooling/warming anomalies in the southwest, southeast, and east sectors likely arise from localized enhancements, such as the convergence of lake breezes with the background southwesterly flow and interactions with heterogeneous land surfaces, which amplify the thermal signal. In contrast, the farthest propagation along the north-south axis is primarily governed by the persistent advection of lake-modified air masses by the dominant background wind. This demonstrates that while local processes determine the intensity of the lake effect, the background circulation ultimately controls its spatial extent.

3.3. Mechanism of lake effect propagation

To explain the mechanisms governing the spatial propagation of lake thermal effects, we analyze both the background atmospheric circulation (Fig. 8) and lake-induced modifications of atmospheric circulation (Figs. 9–12). The composite surface wind and pressure fields reveal persistent southwesterly flow dominance over Poyang Lake under both daytime and nighttime conditions, with enhanced wind speeds during nighttime (particularly over the lake surface). A pronounced high-pressure anomaly develops over the lake and adjacent Yangtze River floodplains, exhibiting notable diurnal variation in spatial extent. The nighttime high-pressure system expands significantly compared to its daytime counterpart. The consistent southwesterly flow orientation across all observed levels facilitates advection of lake-modified air masses toward north region, while topographic channeling along the Yangtze valley appears to enhance this transport. These circulation patterns collectively account for several observed thermal features: (1) persistent southwesterlies drive downwind advection of lake effects, generating the asymmetric thermal distributions shown in Fig. 7; (2) nighttime wind acceleration enhances vertical mixing, directly enabling the broader spatial propagation of warming evident in Fig. 3b. The coordinated action of horizontal advection governs both the directional preference and spatial scale of lake-atmosphere interactions.

Analysis of wind fields across multiple pressure levels (Supplementary Fig. S11) demonstrates systematic clockwise rotation with height, indicating strong coupling between surface and upper-level atmospheric processes. The lower troposphere (850 hPa) is predominantly influenced by southwesterly flows, while the mid-troposphere (500 hPa) exhibits transitional characteristics with combined southwesterly and westerly components. A notable directional shift occurs in the upper troposphere (200 hPa), where northeasterlies emerge as the dominant flow pattern, surpassing the prevalence of westerly winds. This vertical wind structure aligns with observed lake-induced thermal patterns (Figs. 3 and 4), revealing coordinated surface-upper atmosphere interactions that govern the spatial propagation of lake effects.

The investigation of atmospheric circulation responses to lake regulation reveals significant modifications in both horizontal and vertical pressure and wind fields that either amplify or suppress the propagation of lake effects. Horizontally, the lake induces a distinct surface low-pressure trough northwest of its location, markedly enhancing southerly wind anomalies over the water body, with this phenomenon being particularly pronounced during daytime hours (Fig. 9).

The spatial propagation of lake effects is governed by an interplay between background wind fields and diurnally varying circulations across multiple atmospheric levels (Fig. 10). During daytime, the 850 hPa circulation pattern exhibits a pronounced geopotential height depression over the lake contrasting with surrounding highs, generating strong northwesterly wind anomalies. Nighttime conditions reverse this pattern, with the lake developing elevated geopotential heights similar to adjacent land areas, thereby weakening northwesterly flows. While these lake-land contrasts disappear at 500 hPa and 200 hPa levels, replaced by a persistent low-pressure center north of the lake, the characteristic northwesterly anomalies maintain their presence throughout the vertical column.

The observed attenuation scales quantitatively manifest the

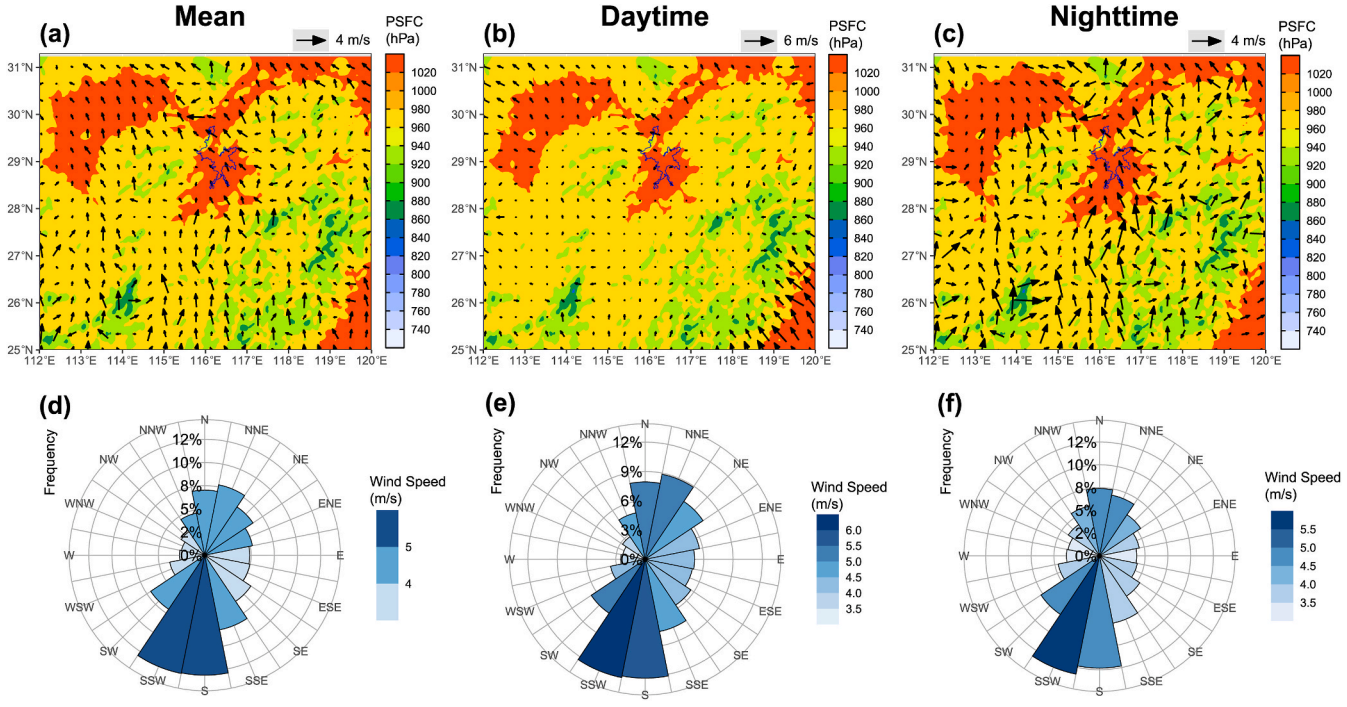

Fig. 8. Near-surface atmospheric circulation: (first row) average surface pressure (PSFC, hPa; shaded) and 10-m wind (m/s; vector) for (a) entire simulation period, (b) typical daytime hour (15:00 local time), and (c) typical nighttime hour (06:00 local time). (d–f) Frequencies of 10-m wind backgrounds directions and average speeds (16 directional sectors) for (d) entire period, (e) daytime, and (f) nighttime. Data is derived from CTRL simulation outputs. The blue frame outlines the boundary of Poyang Lake.

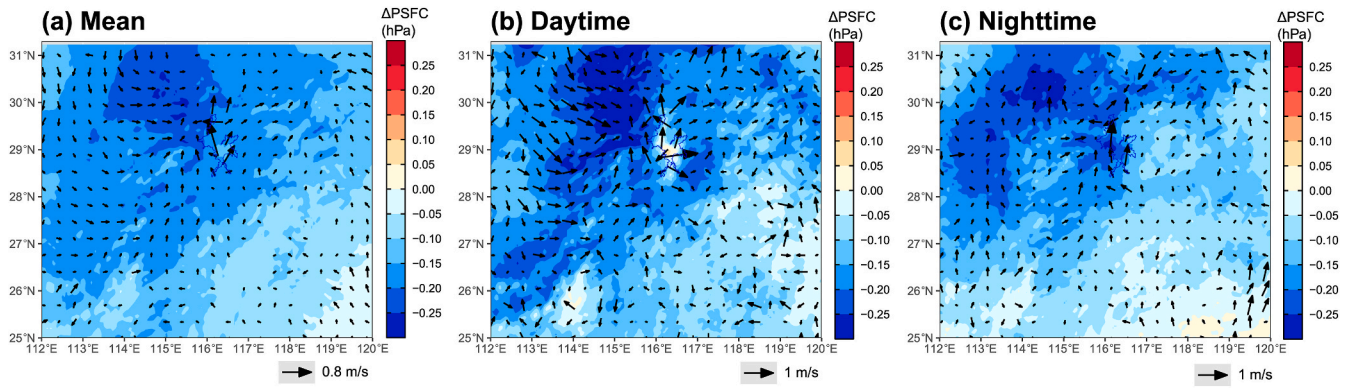

Fig. 9. Lake-induced surface pressure (shaded, hPa) and 10-m wind (vector, m/s) differences for (a) entire simulation period, (b) typical daytime hour (15:00 local time), and (c) typical nighttime hour (06:00 local time). The blue frame outlines the boundary of Poyang Lake.

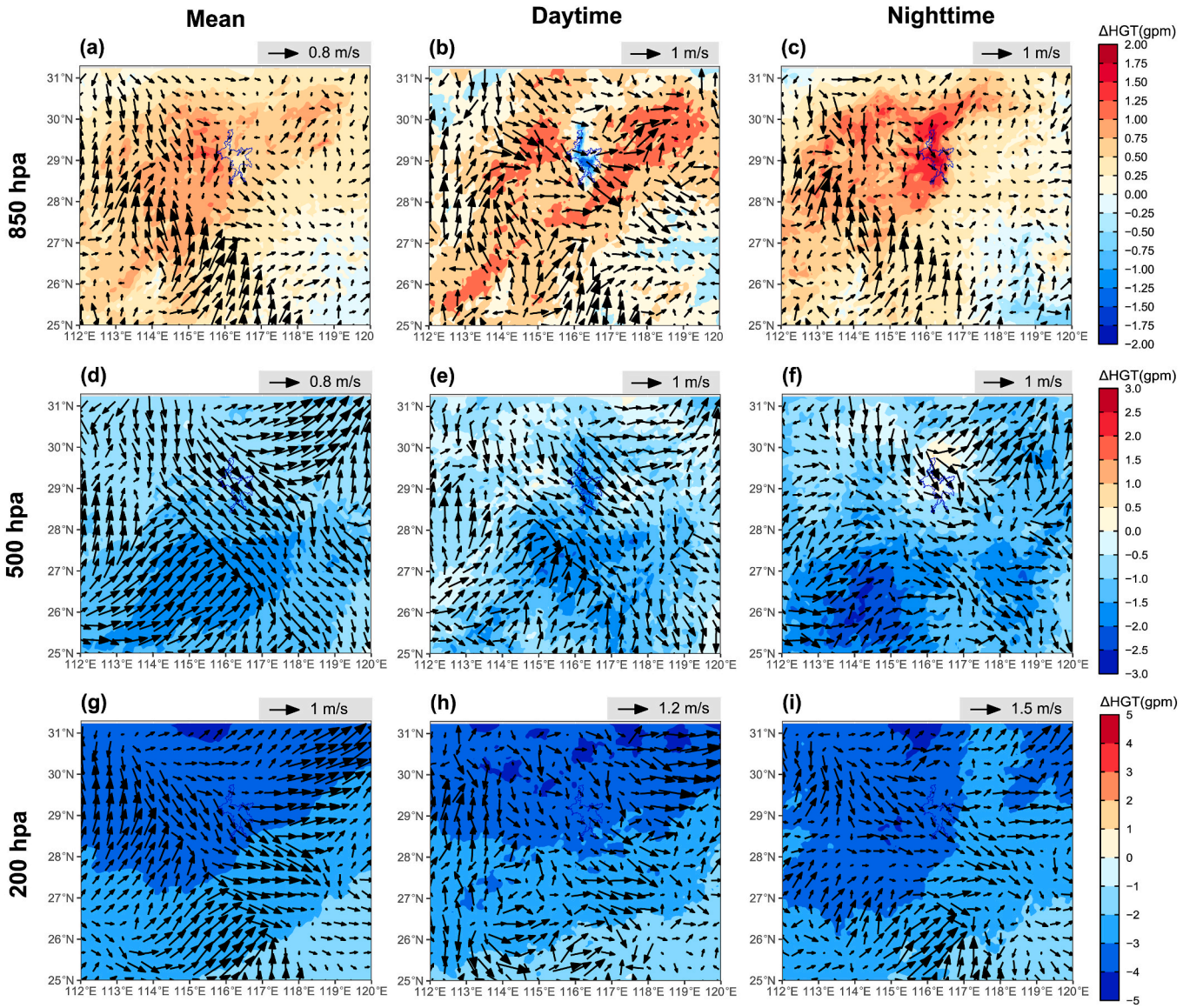

Fig. 10. Lake-induced atmospheric circulation differences: geopotential height (shaded, gpm) and horizontal winds (vector, m/s) at pressure level of (first row) 850 hPa, (second row) 500 hPa, and (third row) 200 hPa for (left column) entire simulation period, (center column) typical daytime hour (15:00 local time), and (right column) typical nighttime hour (06:00 local time). The blue frame outlines the boundary of Poyang Lake.

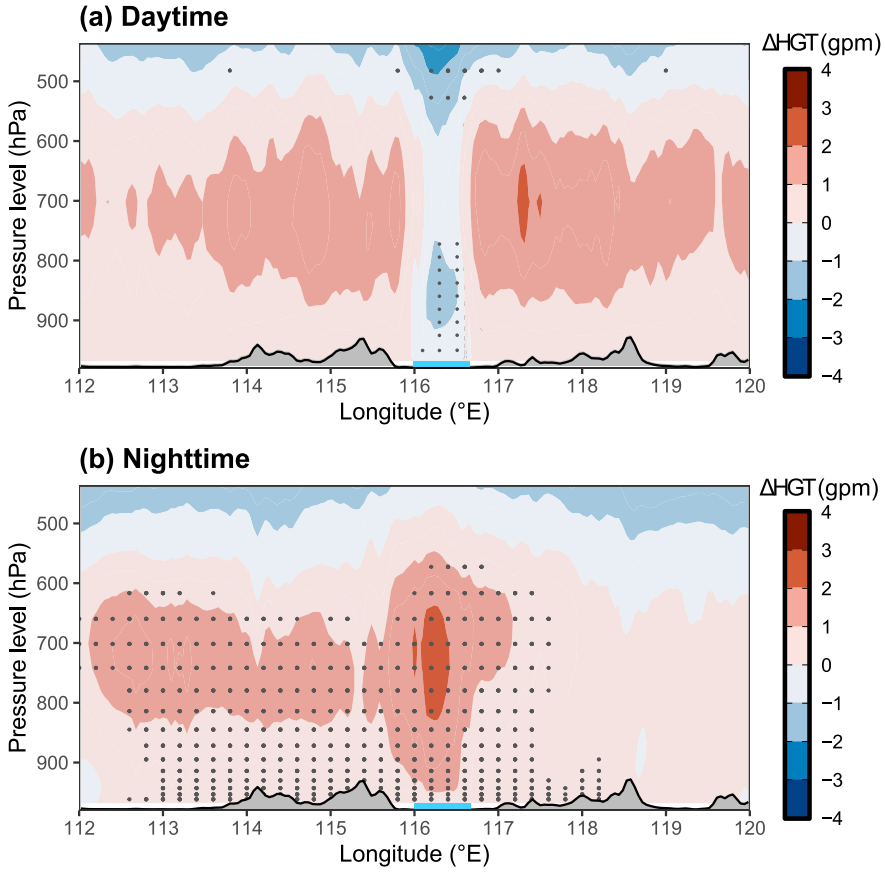

Fig. 11. West-East cross section at 29°N of lake-induced geopotential height (shaded, gpm) differences at (a) typical daytime hour (15:00 local time) and (b) typical nighttime hour (06:00 local time). Dots denote grid cells where differences are significant at the 95 % significance level using a two-sided Student's *t*-test based on daily time series. All values represent the average differences during the simulation. The gray shaded area represents the terrain height, and the blue bold line denotes the location of Poyang Lake.

equilibrium between wind-driven advection (controlling directionality) and thermodynamic dissipation (regulating spatial extent). This balance is further modulated by topographic channeling effects that enhance downstream transport along the Yangtze floodplain. The persistent northwesterly anomalies across all levels, coupled with diurnally alternating pressure systems near the surface, create a vertically coherent mechanism that sustains lake-effect propagation while maintaining its directional preference. The vertical decoupling of pressure systems (surface variability vs. upper-level consistency) suggests that while lake-forced circulations dominate boundary layer processes, their climatic impacts are ultimately constrained by synoptic-scale patterns aloft.

From a vertical perspective, the horizontal pressure gradients induced by lake thermal regulation drive notable advective changes (Figs. 11 and 12). An anomalous low-pressure system develops below 500 hPa over the lake during daytime, confined by surrounding thermal highs and vertically connected to upper-level low-pressure layers (Fig. 11a). This daytime pressure anomaly stems from substantial lake-induced cooling effects that stabilize the lower atmosphere and generate anomalous subsidence. Conversely, nighttime lake warming establishes an anomalous high-pressure system that extends beyond the lake area rather than remaining confined above it (Fig. 11b). This high-pressure system exhibits northward expansion under the influence of prevailing southerly background flows.

Vertical circulation reveals distinct diurnal patterns in lake-atmospheric interactions (Fig. 12). During daytime, rapid land surface heating establishes a thermal low-pressure system, while the relatively cooler lake maintains higher pressure, driving cold air flow from the water body toward surrounding land areas (Fig. 12a). Intense surface warming creates an unstable boundary layer characterized by strong turbulent mixing, which rapidly dilutes the lake-cooled air mass and limits its spatial extent. The shallow lake-induced cold air layer interacts with deeper terrestrial convective mixing, where ascending warm air currents disrupt and dissipate the cooling influence, preventing sustained propagation of temperature modifications.

Nighttime conditions exhibit contrasting dynamics, as the lake continuously releases longwave radiation to warm near-surface air while the land rapidly cools, forming a cold high-pressure system that generates a land breeze (Fig. 12b). This circulation achieves considerable spatial influence (>50 km) due to stable boundary layer conditions. The nighttime temperature inversion effectively suppresses turbulent mixing, allowing horizontal diffusion of lake-generated heat to produce more persistent and extensive warming effects compared to daytime conditions.

The diagnostic analysis of surface energy components provides quantitative evidence for the proposed mechanisms governing the diurnal asymmetry in lake effect propagation (Supplementary Fig. S12). For the daytime period, the significantly negative lake-induced difference in planetary boundary layer height (PBLH) coupled with strongly negative latent heat flux (LHF) and sensible heat flux (SHF). While this creates a near-surface cool pool, the suppressed PBLH acts to confine this cooling effect by inhibiting vertical mixing, thereby preventing its extensive horizontal spread. In contrast, during the nighttime, the positive differences in both SHF and LHF confirm that the lake continuously releases stored energy to warm the overlying air. The relatively small

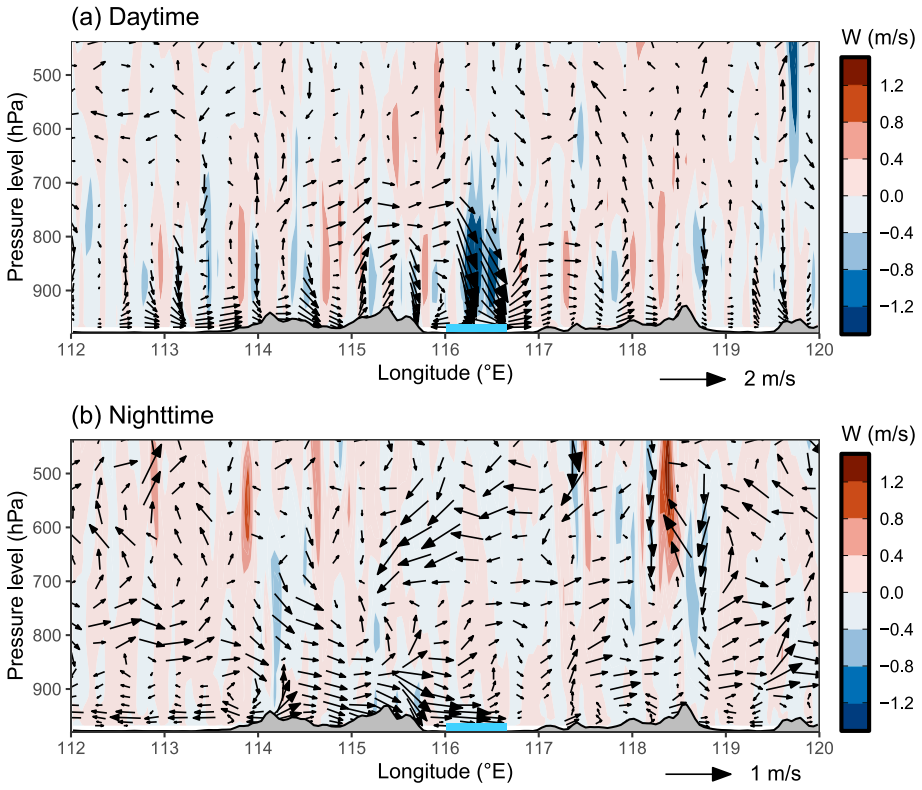

Fig. 12. West-East cross section at 29°N of lake-induced vertical velocity (W, shaded, m/s) and zonal circulation (vector, m/s) differences at (a) typical daytime hour (15:00 local time) and (b) typical nighttime hour (06:00 local time). All values represent the average differences during the simulation. The gray shaded area represents the terrain height, and the blue bold line denotes the location of Poyang Lake. The vertical velocity is amplified 50 times for better illustration.

magnitude of the PBLH difference indicates a persistently stable atmospheric stratification near the surface, which effectively suppresses turbulent dissipation. This stable environment, combined with the sustained energy supply from the lake surface (evidenced by the strong positive upward longwave radiation difference), favors the horizontal advection of the warm air masses. Consequently, the lake-induced warming influence can propagate over a much greater distance downwind than its daytime cooling counterpart.

In summary, the spatial propagation of lake effects is primarily governed by background wind fields that determine their directional characteristics, while lake-induced modifications of local thermal environments create distinct diurnal circulation patterns. These thermally driven processes lead to significant differences in the spatial extent and attenuation rates between daytime cooling and nighttime warming effects. The key mechanisms include: (1) enhanced turbulent mixing during daytime that weakens and confines lake cooling effects, and (2) stable nighttime atmospheric stratification and enhanced advection that extends lake warming influences. This fundamental diurnal asymmetry arises from differential energy partitioning between shortwave radiation driven evaporative cooling (daytime) and longwave radiation release (nighttime), modulated by the contrasting boundary layer stability conditions characteristic of each period. The combined action of these mechanisms produces the observed spatial variability in lake-atmosphere interactions.

4. Discussion

The pronounced spatial attenuation of lake-effect thermal propagation under extreme heat, as quantified in this study, reveals fundamental characteristics of inland lakes in modulating regional climate extremes. Our findings demonstrate a distinct distance-decay pattern, with daytime cooling effects attenuating within 40 km and nighttime warming persisting up to 70 km from Poyang Lake's shoreline. This spatial gradient aligns with but extends previous studies from other lakes. For example, propagation distances of 10–20 km for the Taihu Lake (Gu et al., 2016) and Miyun Reservoir (Qin et al., 2023) during heatwaves. In contrast, larger water bodies exhibit substantially greater reach: Qinghai Lake's cooling can influence areas 30–100 km downwind (Li et al., 2019), while the impact of Lake Victoria extends approximately 60 km along the prevailing wind direction (Thiery et al., 2015). Most illustrative is the gradient observed across 11 boreal lakes in western Canada, where the temperature buffer potential scales directly with lake surface area, ranging from 10 km to 100 km (Hillman and Nielsen, 2025). Our results provide the first comprehensive quantification for a large lake under unprecedented heat stress. The enhanced nighttime warming range results from the extreme thermal contrast between the persistent warm lake surface and rapidly cooling surrounding lands during the 2022 record heatwave, creating stronger pressure gradients that drive more extensive atmospheric mixing. The identification of characteristic attenuation scales (40 km daytime, 70 km nighttime) provides critical parameters for improving lake representation in regional climate models, which have traditionally underestimated these propagation distances due to coarse resolutions and simplified lake-atmosphere coupling schemes (Zhu et al., 2020).

The directional preference of north-oriented propagation aligns with the prevailing southerly wind patterns in the region, reinforcing the role of background atmospheric circulation in shaping lake-effect distributions. Similar directional biases have been observed in other lake systems, such as Lake Taihu (Sijia et al., 2019) and Lake Victoria (Vanderkelen et al., 2018), though the specific attenuation rates (0.28 °C/10 km daytime, 0.13 °C/10 km nighttime) provide new quantitative insights for the Poyang Lake basin. The vertical penetration of lake effects to 700–900 hPa further demonstrates that lakes influence not only surface conditions but also atmospheric processes, further affecting cloud formation and precipitation patterns downwind (Qiu et al., 2025).

The mechanisms driving these spatial patterns involve complex interactions between lake surface fluxes, atmospheric stability, and lake-induced atmospheric circulation (Rouse et al., 2008). Daytime cooling is limited by turbulent mixing and rapid dissipation of cold air advection, while nighttime warming benefits from stable boundary-layer conditions that suppress vertical mixing and allow horizontal heat diffusion (Gu et al., 2015). These findings are consistent with recent modeling studies (Huang et al., 2017; Wei et al., 2025) but extend their applicability to extreme heat scenarios, where lake effects may be amplified by heightened thermal contrasts between water and land surfaces (Shi et al., 2022).

These findings significantly advance our understanding of inland water bodies as thermal buffers under climate change, where both heatwave intensity and lake surface temperatures are projected to increase (Wang et al., 2024a,b; Woolway et al., 2021). The identification of characteristic propagation scales and attenuation thresholds provides not only fundamental parameters for improving lake representation in regional climate models but also a quantitative framework for guiding future research. Specifically, future studies should investigate how these spatial metrics are influenced by dynamic lake morphometry, hydrological extremes, and broader climatic regimes to build a more generalizable theory of lake-mediated climate feedback.

On a practical level, the quantified propagation gradients offer actionable insights for regional climate adaptation policy. The demonstrated efficacy of large lakes like Poyang Lake as natural thermal buffers underscores the necessity of integrating blue infrastructure into long-term planning in densely populated regions (Cheng et al., 2023). Urban planning strategies, particularly in heat-vulnerable areas, can utilize the 40-km and 70-km influence zones to delineate priority areas for preserving natural water bodies, designing cooling corridors, and mitigating urban heat island effects (Le Phuc et al., 2022). This study underscores the growing importance of integrating inland water bodies into climate resilience policy as their thermal regulatory role becomes increasingly critical under global warming.

This modeling study is subject to several limitations. First, our experimental design involves simplifications that may affect the results. The WRF model, in its standard configuration, cannot represent dynamically changing surface conditions. Therefore, we treat Poyang Lake as a static water body in our simulations. Moreover, in the NOLA experiment, the lake is uniformly replaced with cropland, the dominant land use type in the surrounding region. In reality, the 2022 extreme drought caused significant lake shrinkage, which likely alters lake-atmosphere interaction processes. Furthermore, the actual land cover surrounding the lake is a complex mosaic including forests, wetlands, and urban areas (Yang et al., 2025). Using cropland as the sole substitute may therefore exaggerate the lake-land contrast. Second, the sparse distribution of meteorological stations around Poyang Lake limits the observational validation of the fine-scale spatial gradients. This observational gap reduces our ability to fully capture localized microclimatic variations that may influence the lake's thermal regulation capacity. Additionally, the lack of long-term, high-resolution measurements over the lake surface hinders precise validation of the model's representation of critical lake-atmosphere exchange processes during extreme heat. These limitations highlight the need for enhanced monitoring networks to better constrain lake-atmosphere interactions in future studies. In addition, future simulation research should explore how lake morphology (e.g., depth, shape) and hydrological changes (e.g., seasonal water area changes) modulate thermal propagation dynamics. The potential feedback between lake effects and larger-scale atmospheric processes, such as monsoon circulation, warrants further investigation.

It is important to note that our findings characterize lake thermal propagation specifically during an extreme heat event. The identified attenuation scales and intensities may differ under moderate climatic conditions due to variations in background wind speed, atmospheric stability, and land-lake thermal contrast. Future research should include comparative simulations of both extreme and non-extreme years to quantify how these dynamics shift across a gradient of climatic forcing.

5. Conclusions

Lakes are well-established thermal regulators that mitigate extreme heat. However, the spatial extent and propagation mechanisms of lake thermal regulation remain unresolved due to complex lake-atmosphere couplings. This study provides a comprehensive analysis of the spatial propagation and physical mechanisms governing lake-induced thermal regulation during extreme heat based on WRF simulations, as exemplified by the largest freshwater Poyang Lake (China). The results demonstrate pronounced diurnal asymmetry in the lake's climatic influence, characterized by strong daytime cooling constrained within 40 km of the boundary and more extensive nighttime warming reaching up to 70 km. The attenuation rates of 0.28 °C/10 km (daytime) and 0.13 °C/10 km (nighttime) are correspondingly detected. In terms of vertical profile, lake effects penetrate to approximately 700–900 hPa, with daytime effects concentrated near the surface and nighttime impacts showing greater horizontal extent under stable boundary-layer conditions. The spatial propagation of lake effects exhibits clear directional preference, with north-oriented attenuation shaped by prevailing southerly winds and modified by local thermal circulations.

These contrasting patterns arise from fundamental differences in energy exchange processes. Daytime cooling is primarily driven by evaporative heat loss and limited by turbulent mixing with warmer surrounding air, while nighttime warming benefits from stable atmospheric conditions that enhance the horizontal diffusion of heat released through longwave radiation.

This work establishes lakes as active participants in regional climate systems and contributes a framework for assessing their role in modulating temperature extremes under global warming. This study highlights the growing importance of integrating inland water bodies into climate resilience planning, as their thermal regulatory role becomes increasingly critical under continued warming. Future studies should investigate how the identified spatial metrics are influenced by dynamic lake morphometry, hydrological extremes, and broader climatic regimes to build a more generalizable theory of lake-mediated climate feedback.

CRediT authorship contribution statement

Zikang Xing: Writing – original draft, Visualization, Validation, Methodology, Investigation, Formal analysis, Data curation. **Yunliang Li:** Supervision, Funding acquisition. **Yufeng Dai:** Supervision. **Jianhui Wei:** Writing – review & editing, Supervision. **Miaomiao Ma:** Resources, Project administration. **Xuejun Zhang:** Supervision, Resources. **Hui Gao:** Funding acquisition. **Harald Kunstmann:** Supervision, Project administration.

Declaration of competing interest

The authors declare that they have no known competing financial interests or personal relationships that could have appeared to influence the work reported in this paper.

Acknowledgments

This work was supported by the National Key Research and Development Program of China (2023YFC3206001), the National Natural Science Foundation of China (42401049), the China Postdoctoral Science Foundation (2024M763367), the Jiangxi Provincial Natural Science Foundation (20252BAC200244), the Science Foundation of Nanjing Institute of Geography and Limnology, Chinese Academy of Sciences (NIGLAS2022GS08), the Youth Innovation Promotion Association of the Chinese Academy of Sciences (Y2023084, 2022067), the Key Program of Natural Science Foundation of Jiangxi Province (20242BAB26044), the Jiangxi "Double Thousand Plan"

(jxsq2023101105), the IWHR Internationally-Oriented Talent for International Academic Leader Program (0203982012), and the BMFTR funded KARE_II project (01LR2006D1).

Appendix A. Supplementary data

Supplementary data to this article can be found online at https://doi.org/10.1016/j.wace.2025.100847.

Data availability

Data will be made available on request.

References

Adrian, R., O'Reilly, C.M., Zagarese, H., Baines, S.B., Hessen, D.O., Keller, W., Livingstone, D.M., Sommaruga, R., Straile, D., Van Donk, E., Weyhenmeyer, G.A., Winder, M., 2009. Lakes as sentinels of climate change. Limnol. Oceanogr. 54, 2283–2297, 10/cg4884.

Bennington, V., Notaro, M., Holman, K.D., 2014. Improving climate sensitivity of deep Lakes within a regional climate model and its impact on simulated climate. J. Clim. 27, 2886–2911. https://doi.org/10.1175/JCLI-D-13-00110.1.

Betts, A.K., 1986. A new convective adjustment scheme. Part I: observational and theoretical basis. Q. J. R. Meteorol. Soc. 112, 677–691. https://doi.org/10.1002/qj.49711247307.

Betts, A.K., Miller, M.J., 1986. A new convective adjustment scheme. Part II: single column tests using GATE wave, BOMEX, ATEX and arctic air-mass data sets. Q. J. R. Meteorol. Soc. 112, 693–709. https://doi.org/10.1002/qj.49711247308.

Chen, F., Dudhia, J., 2001. Coupling an advanced land surface–hydrology model with the penn State–NCAR MM5 modeling system. Part I: model implementation and sensitivity. Mon. Wea. Rev. 129, 569–585, 10/c6m89k.

Cheng, Y., Bartesaghi-Koc, C., Tian, Y., Shen, L., Teng, M., Liu, H., Xiao, Z., Zhang, B., Wu, C., 2023. Where and how to cool through blue infrastructure? Large lake groups to ameliorate urban overheating in a typical inland multi-lake megacity. Sustain. Cities Soc. 98, 104869, 10/gtpggr.

Collazo, S., Suli, S., Zaninelli, P.G., García-Herrera, R., Barriopedro, D., Garrido-Perez, J. M., 2024. Influence of large-scale circulation and local feedbacks on extreme summer heat in Argentina in 2022/23. Commun. Earth Environ. 5, 231. https://doi.org/10.1038/s43247-024-01386-8.

Cremona, A., Huss, M., Landmann, J.M., Borner, J., Farinotti, D., 2023. European heat waves 2022: contribution to extreme glacier melt in Switzerland inferred from automated ablation readings. Cryosphere 17, 1895–1912. https://doi.org/10.5194/tc-17-1895-2023.

Dai, Y., Chen, D., Yao, T., Wang, L., 2020. Large lakes over the Tibetan Plateau may boost snow downwind: implications for snow disaster. Sci. Bull. 65, 1713–1717. https://doi.org/10.1016/j.scib.2020.06.012.

Defourny, P., Bontemps, S., Lamarche, C., Brockmann, C., Boettcher, M., Wevers, J., Kirches, G., 2017. Land Cover CCI: Product User Guide Version 2.0.

Dudhia, J., 1989. Numerical Study of Convection Observed During the Winter Monsoon Experiment Using a Mesoscale Two-Dimensional Model.

Gu, H., Jin, J., Wu, Y., Ek, M.B., Subin, Z.M., 2015. Calibration and validation of lake surface temperature simulations with the coupled WRF-lake model. Clim. Change 129, 471–483. https://doi.org/10.1007/s10584-013-0978-y.

Gu, H., Ma, Z., Li, M., 2016. Effect of a large and very shallow lake on local summer precipitation over the Lake Taihu basin in China. J. Geophys. Res. Atmos. 121, 8832–8848, 10/gtgjk2.

Hersbach, H., Bell, B., Berrisford, P., Hirahara, S., Horányi, A., Muñoz-Sabater, J., Nicolas, J., Peubey, C., Radu, R., Schepers, D., Simmons, A., Soci, C., Abdalla, S., Abellan, X., Balsamo, G., Bechtold, P., Biavati, G., Bidlot, J., Bonavita, M., De Chiara, G., Dahlgren, P., Dee, D., Diamantakis, M., Dragani, R., Flemming, J., Forbes, R., Fuentes, M., Geer, A., Haimberger, L., Healy, S., Hogan, R.J., Hólm, E., Janisková, M., Keeley, S., Laloyaux, P., Lopez, P., Lupu, C., Radnoti, G., De Rosnay, P., Rozum, I., Vamborg, F., Villaume, S., Thépaut, J., 2020. The ERA5 global reanalysis. Q. J. R. Meteorol. Soc. 146, 1999–2049. https://doi.org/10.1002/qj.3803.

Hillman, A., Nielsen, S.E., 2025. Climate buffering effects of western Canadian boreal lakes: the effect of lake size and depth on shoreline and nearshore forests. Landsc. Ecol. 40, 124. https://doi.org/10.1007/s10980-025-02146-5.

Hong, S.-Y., Dudhia, J., Chen, S.-H., 2004. A revised approach to ice microphysical processes for the bulk parameterization of clouds and precipitation. Mon. Wea. Rev. 132, 103–120. https://doi.org/10.1175/1520-0493(2004)132<0103:ARATIM>2.0.CO;2.

Hong, S.-Y., Noh, Y., Dudhia, J., 2006. A new vertical diffusion package with an explicit treatment of entrainment processes. Mon. Weather Rev. 134, 2318–2341. https://doi.org/10.1175/MWR3199.1.

Hostetler, S.W., Bartlein, P.J., 1990. Simulation of lake evaporation with application to modeling lake level variations of Harney-Malheur Lake, Oregon. Water Resour. Res. 26, 2603–2612, 10/d3prz8.

Hostetler, S.W., Bates, G.T., Giorgi, F., 1993. Interactive coupling of a lake thermal model with a regional climate model. J. Geophys. Res. Atmos. 98, 5045–5057, 10/d6g5zv.

Hostetler, S.W., Giorgi, F., Bates, G.T., Bartlein, P.J., 1994. Lake-Atmosphere feedbacks associated with paleolakes bonneville and Lahontan. Science 263, 665–668. https://doi.org/10.1126/science.263.5147.665.

Huang, L., Wang, J., Zhu, L., Ju, J., Daut, G., 2017. The warming of large Lakes on the Tibetan Plateau: evidence from a Lake model simulation of Nam Co, China, during 1979–2012. JGR Atmosph. 122. https://doi.org/10.1002/2017JD027379.

Huntingford, C., Cox, P.M., Ritchie, P.D.L., Clarke, J.J., Parry, I.M., Williamson, M.S., 2024. Acceleration of daily land temperature extremes and correlations with surface energy fluxes. npj Clim. Atmos. Sci. 7, 84. https://doi.org/10.1038/s41612-024-00626-0.

Iakunin, M., Salgado, R., Potes, M., 2018. Breeze effects at a large artificial lake: summer case study. Hydrol. Earth Syst. Sci. 22, 5191–5210. https://doi.org/10.5194/hess-22-5191-2018.

Jach, L., Warrach-Sagi, K., Ingwersen, J., Kaas, E., Wulfmeyer, V., 2020. Land cover impacts on land-atmosphere coupling strength in climate simulations with WRF over Europe. JGR Atmosph. 125, 10/gscc3n. e2019JD031989.

Jiménez, P.A., Dudhia, J., González-Rouco, J.F., Navarro, J., Montávez, J.P., García-Bustamante, E., 2012. A revised scheme for the WRF surface layer formulation. https://doi.org/10.1175/MWR-D-11-00056.1.

Kong, D., Xie, Y., Gu, X., Slater, L., Ci, H., Song, H., 2024. Contribution of anthropogenic activities to the intensification of heat index-based spatiotemporally contiguous heatwave events in China. J. Geophys. Res. Atmos. 129, 10/gtjxvf. e2023JD040004.

Le Phuc, C.L., Nguyen, H.S., Dao Dinh, C., Tran, N.B., Pham, Q.B., Nguyen, X.C., 2022. Cooling island effect of urban lakes in hot waves under foehn and climate change. Theor. Appl. Climatol. 149, 817–830, 10/gtpvnj.

Li, H., Ren, G., Li, W., 2019. Diurnal and intra-season variation of warm-season temperature in coastal zone of Qinghai Lake. Theor. Appl. Climatol. 138, 1203–1217. https://doi.org/10.1007/s00704-019-02893-x.

Li, Y., Tan, Z., Zhang, Q., Liu, X., Chen, J., Yao, J., 2021. Refining the concept of hydrological connectivity for large floodplain systems: framework and implications for eco-environmental assessments. Water Res. 195, 117005. https://doi.org/10.1016/j.watres.2021.117005.

Li, Y., Zhang, Q., Tan, Z., Yao, J., 2020. On the hydrodynamic behavior of floodplain vegetation in a flood-pulse-influenced river-lake system (Poyang Lake, China). J. Hydrol. 585, 124852. https://doi.org/10.1016/j.jhydrol.2020.124852.

Luo, M., Wu, S., Ngar, G., Lau, C., Pei, T., Liu, Z., Wang, X., Ning, G., Chan, T.O., Yang, Y., Zhang, W., 2024. Anthropogenic forcing has increased the risk of longer-traveling and slower-moving large contiguous heatwaves. Sci. Adv. 10. https://doi.org/10.1126/sciadv.adl1598 eadl1598.

Ma, F., Yuan, X., 2023. When will the unprecedented 2022 summer heat waves in Yangtze River Basin become normal in a warming climate? Geophys. Res. Lett. 50, 10/gs9qrc.

Mishra, V., Cherkauer, K.A., Bowling, L.C., 2011. Changing thermal dynamics of lakes in the Great Lakes region: role of ice cover feedbacks. Global Planet. Change 75, 155–172, 10/ckpkb6.

Mlawer, E.J., Taubman, S.J., Brown, P.D., Iacono, M.J., Clough, S.A., 1997. Radiative transfer for inhomogeneous atmospheres: RRTM, a validated correlated-k model for the longwave. J. Geophys. Res. 102, 16663–16682. https://doi.org/10.1029/97JD00237.

Muñoz Sabater, J., 2019. ERA5-Land hourly data from 1950 to present. https://doi.org/10.24381/cds.e2161bac.

Muñoz-Sabater, J., Dutra, E., Agustí-Panareda, A., Albergel, C., Arduini, G., Balsamo, G., Boussetta, S., Choulga, M., Harrigan, S., Hersbach, H., Martens, B., Miralles, D.G., Piles, M., Rodríguez-Fernández, N.J., Zsoter, E., Buontempo, C., Thépaut, J.-N., 2021. ERA5-Land: a state-of-the-art global reanalysis dataset for land applications. Earth Syst. Sci. Data 13, 4349–4383, 10/gnp75m.

Oleson, K., Lawrence, D., Bonan, G., Drewniak, B., Huang, M., Koven, C., Levis, S., Li, F., Riley, W., Subin, Z., Swenson, S., Thornton, P., Bozbiyik, A., Fisher, R., Heald, C., Kluzek, E., Lamarque, J.-F., Lawrence, P., Leung, L., Lipscomb, W., Muszala, S., Ricciuto, D., Sacks, W., Sun, Y., Tang, J., Yang, Z.-L., 2013. Technical Description of Version 4.5 of the Community Land Model (CLM). UCAR/NCAR. https://doi.org/10.5065/D6RR1W7M.

Qin, J., Xing, Y., Liu, J., Nakhaei, P., Hamamy, W., Li, B., Yang, L., Ni, G., 2023. Modelling analysis of the potential impact of large reservoir on heatwave events. Ecol. Indic. 154, 110841. https://doi.org/10.1016/j.ecolind.2023.110841.

Qiu, Y., Chen, J., Chen, D., Li, W., Xiong, L., 2023. Lake-area expansion alters downwind precipitation patterns on the Tibetan Plateau: insights from the Most dramatically expanded Lake. JGR Atmosph. 128. https://doi.org/10.1029/2023JD039274 e2023JD039274.

Qiu, Y., Chen, J., Chen, D., Woolway, R.I., Luo, H., Xiong, L., 2025. Dipolar response of precipitation to lake expansion on the Tibetan Plateau. J. Hydrol. 660, 133532. https://doi.org/10.1016/j.jhydrol.2025.133532.

Rooney, G.G., Bornemann, F.J., 2013. The performance of FLake in the met office unified model. Tellus Dyn. Meteorol. Oceanogr. 65, 21363. https://doi.org/10.3402/tellusa.v65i0.21363.

Rouse, W.R., Blanken, P.D., Bussières, N., Walker, A.E., Oswald, C.J., Schertzer, W.M., Spence, C., 2008. An investigation of the thermal and energy balance regimes of great slave and great bear Lakes. J. Hydrometeorol. 9 (1), 1318–1333. https://doi.org/10.1175/2008JHM977.

Shi, Y., Huang, A., Ma, W., Wen, L., Zhu, L., Yang, X., Wu, Y., Gu, C., 2022. Drivers of warming in Lake Nam Co on Tibetan Plateau over the past 40 years. JGR Atmosph. 127. https://doi.org/10.1029/2021JD036320 e2021JD036320.

Sijia, J., Wei, X., Wei, W., Qiang, L., Zhen, Z., Cheng, H., Xuhui, L., 2019. Evaluation on the performance of CLM4-LISSS in simulating water and heat fluxes at multiple time scales over Lake Taihu. J. Lake Sci. 31, 1698–1712. https://doi.org/10.18307/2019.0611. Yale-NUIST Center on Atmospheric Environment, Nanjing University of

Information Science & Technology, Nanjing 210044, P. R. China;School of Applied Meteorology, Nanjing University of Information Science & Technology, Nanjing 210044, P. R. China.

Skamarock, W.C., Klemp, J.B., Dudhia, J., Gill, D.O., Liu, Z., Berner, J., Wang, W., Powers, J.G., Duda, M.G., Barker, D.M., Huang, X.-Y., 2008. A Description of the Advanced Research WRF Model Version 4.

Sun, J., Lenschow, D.H., Mahrt, L., Crawford, T.L., Davis, K.J., Oncley, S.P., MacPherson, J.I., Wang, Q., Dobosy, R.J., Desjardins, R.L., 1997. Lake-induced atmospheric circulations during BOREAS. J. Geophys. Res. Atmos. 102, 29155–29166, 10/bh82sh.

Sun, X., Xie, L., Semazzi, F.H.M., Liu, B., 2014. A numerical investigation of the precipitation over Lake Victoria basin using a coupled atmosphere-lake limited-area model. Adv. Meteorol. 2014, 960924. https://doi.org/10.1155/2014/960924.

Thiery, W., Davin, E.L., Panitz, H.-J., Demuzere, M., Lhermitte, S., Van Lipzig, N., 2015. The impact of the African Great Lakes on the regional climate. J. Clim. 28, 4061–4085. https://doi.org/10.1175/JCLI-D-14-00565.1.

Tsujimoto, K., Koike, T., 2013. Land-lake breezes at low latitudes: the case of Tonle Sap Lake in Cambodia. JGR Atmosph. 118, 6970–6980. https://doi.org/10.1002/jgrd.50547.

Ueno, K., Ohta, S., 2020. Effects of changes in land use on the diurnal temperature range: a long-term data analysis. Environ. Res. Commun. 2, 021001. https://doi.org/10.1088/2515-7620/ab67ef.

Vanderkelen, I., Van Lipzig, N.P.M., Sacks, W.J., Lawrence, D.M., Clark, M.P., Mizukami, N., Pokhrel, Y., Thiery, W., 2021. Simulating the impact of global reservoir expansion on the present-day climate. JGR Atmosph. 126, 10/gsfp5n e2020JD034485.

Vanderkelen, I., Van Lipzig, N.P.M., Thiery, W., 2018. Modelling the water balance of Lake Victoria (East Africa) – part 1: observational analysis. Hydrol. Earth Syst. Sci. 22, 5509–5525, 10/gfjngt.

Von Schuckmann, K., Minère, A., Gues, F., Cuesta-Valero, F.J., Kirchengast, G., Adusumilli, S., Straneo, F., Allan, R., Barker, P.M., Beltrami, H., Boyer, T., Cheng, L., Church, J., Desbruyeres, D., Dolman, H., Domingues, C.M., García-García, A., Giglio, D., Gilson, J.E., Gorfer, M., Haimberger, L., Hendricks, S., Hosoda, S., Johnson, G.C., Killick, R., King, B., Kolodziejczyk, N., Korosov, A., Krinner, G., Kuusela, M., Langer, M., Lavergne, T., Lawrence, I., Li, Y., Lyman, J., Marzeion, B., Mayer, M., MacDougall, A.H., McDougall, T., Monselesan, D.P., Nitzbon, J., Otosaka, I., Peng, J., Purkey, S., Roemmich, D., Sato, Kanako, Sato, Katsunari, Savita, A., Schweiger, A., Shepherd, A., Seneviratne, S.I., Simons, L., Slater, D.A., Slater, T., Smith, N., Steiner, A., Suga, T., Szekely, T., Thiery, W., Timmermans, M.-L., Vanderkelen, I., Wjiffels, S.E., Wu, T., Zemp, M., 2022. Heat stored in the Earth system 1960–2020: where does the energy go? https://doi.org/10.5194/essd-2022-239.

Wagner, S., Fersch, B., Yuan, F., Yu, Z., Kunstmann, H., 2016. Fully coupled atmospheric-hydrological modeling at regional and long-term scales: development, application, and analysis of WRF-HMS. Water Resour. Res. 52, 3187–3211. https://doi.org/10.1002/2015WR018185.

Wan, Z., Hook, S., Hulley, G., 2015. MOD11A1 MODIS/terra land surface temperature/emissivity daily L3 global 1km SIN grid V006. https://doi.org/10.5067/MODIS/MOD11A1.006.

Wang, B., Ma, Y., Wang, Y., Su, Z., Ma, W., 2019. Significant differences exist in lake-atmosphere interactions and the evaporation rates of high-elevation small and large lakes. J. Hydrol. 573, 220–234, 10/gnxvfw.

Wang, F., Ni, G., Riley, W.J., Tang, J., Zhu, D., Sun, T., 2019. Evaluation of the WRF lake module (v1.0) and its improvements at a deep reservoir. Geosci. Model Dev. (GMD) 12, 2119–2138, 10/gtb732.

Wang, J., Xue, P., Pringle, W., Yang, Z., Qian, Y., 2022. Impacts of Lake surface temperature on the summer climate over the Great Lakes region. J. Geophys. Res. Atmos. 127. https://doi.org/10.1029/2021JD036231 e2021JD036231.

Wang, W., Shi, K., Wang, X., Zhang, Yunlin, Qin, B., Zhang, Yibo, Woolway, R.I., 2024. The impact of extreme heat on lake warming in China. Nat. Commun. 15, 70, 10/gtb844.

Wang, X., Shi, K., Qin, B., Zhang, Y., Woolway, R.I., 2024. Disproportionate impact of atmospheric heat events on lake surface water temperature increases. Nat. Clim. Chang. https://doi.org/10.1038/s41558-024-02122-y.

Wang, X., Zhang, Z., Zhang, B., Tian, L., Tian, J., Arnault, J., Kunstmann, H., He, C., 2023. Quantifying the impact of land use and land cover change on moisture recycling with convection-permitting WRF-Tagging modeling in the agro-pastoral ecotone of Northern China. JGR Atmosph. 128, 10/gspvsx e2022JD038421.

Wei, J., Arnault, J., Rummler, T., Fersch, B., Zhang, Z., Olschewski, P., Laux, P., Dong, N., Yang, Q., Xing, Z., Li, X., Yang, C., Zhang, X., Ma, M., Gao, L., Xu, L., Yu, Z., Kunstmann, H., 2024. Acceleration of the hydrological cycle under global warming for the Poyang Lake Basin in Southeast China: an age-weighted regional water tagging approach. J. Hydrometeorol. 25, 1627–1647. https://doi.org/10.1175/JHM-D-23-0227.1.

Wei, Jianhui, Dong, N., Arnault, J., Fersch, B., Wagner, S., Zhang, Z., Laux, P., Yang, C., Yang, Q., Yu, Z., Kunstmann, H., 2020. How reservoir regulation modifies the regional terrestrial-atmospheric water cycle: incorporation of a reservoir network module into a fully-coupled hydrological-atmospheric model (other). Oral. https://doi.org/10.5194/egusphere-egu2020-16219.

Wei, J., Wang, W., Cao, M., Zhang, J., Jin, J., Wang, G., Li, H., Pan, X., Ye, Z., Teuling, A. J., Wang, S., 2025. Has the three gorges reservoir impacted regional moisture recycling? Water Resour. Res. 61. https://doi.org/10.1029/2024WR038208 e2024WR038208.

Wei, Jia, Wang, W., Shao, Q., Yu, Z., Chen, Z., Huang, Y., Xing, W., 2020. Heat wave variations across China tied to global SST modes. JGR Atmosph. 125. https://doi.org/10.1029/2019JD031612 e2019JD031612.

Woolway, R.I., Jennings, E., Shatwell, T., Golub, M., Pierson, D.C., Maberly, S.C., 2021. Lake heatwaves under climate change. Nature 589, 402–407. https://doi.org/10.1038/s41586-020-03119-1.

Woolway, R.I., Kraemer, B.M., Lenters, J.D., Merchant, C.J., O'Reilly, C.M., Sharma, S., 2020. Global lake responses to climate change. Nat. Rev. Earth Environ. 1, 388–403, 10/gg6tzz.

Xing, Z., Wei, J., Li, Y., Zhang, X., Ma, M., Yi, P., Ju, Q., Laux, P., Kunstmann, H., 2024. Disentangling the spatially combined and temporally lagged influences of climate oscillations on seasonal droughts in the East Asian monsoon influenced Poyang Lake Basin. Atmos. Res. 310, 107603. https://doi.org/10.1016/j.atmosres.2024.107603.

Yang, Q., Wei, J., Wu, L., Yang, C., Li, L., Luo, J., Chen, C., Gu, H., Xiao, M., Wang, Q., Kunstmann, H., Yu, Z., 2025. Contribution of climate change and human activities to streamflow and lake water level variations at regional scales. J. Water Clim. Chang. https://doi.org/10.2166/wcc.2025.063.

Zhang, D., Chen, L., Yuan, Y., Zuo, J., Ke, Z., 2023. Why was the heat wave in the Yangtze River valley abnormally intensified in late summer 2022? Environ. Res. Lett. 18, 034014. https://doi.org/10.1088/1748-9326/acba30.

Zhang, Q., Jin, J., Budy, P., Null, S.E., Wang, X., Pennock, C.A., 2021. Predicting thermal responses of an Arctic Lake to whole-lake warming manipulation. Geophys. Res. Lett. 48, 10/gn93zc e2021GL092680.

Zhou, J., Leavitt, P.R., Rose, K.C., Wang, X., Zhang, Y., Shi, K., Qin, B., 2023. Controls of thermal response of temperate lakes to atmospheric warming. Nat. Commun. 14, 6503, 10/gs2575.

Zhu, L., Jin, J., Liu, X., Tian, L., Zhang, Q., 2018. Simulations of the impact of Lakes on local and regional climate over the Tibetan Plateau. Atmos.-Ocean 56, 230–239. https://doi.org/10.1080/07055900.2017.1401524.

Zhu, L., Jin, J., Liu, Y., 2020. Modeling the effects of Lakes in the Tibetan Plateau on diurnal variations of regional climate and their seasonality. J. Hydrometeorol. 21, 2523–2536. https://doi.org/10.1175/JHM-D-20-0091.1.